Interfaces in organic devices studied with resonant soft x-ray reflectivity

Hongping Yan, Cheng Wang, Andres Garcia, Sufal Swaraj, Ziran Gu, Christopher R. McNeill, Torben Schuettfort, Karen E. Sohn, Edward J. Kramer, Guillermo C. Bazan, Thuc-Quyen Nguyen, and Harald Ade

Citation: Journal of Applied Physics **110**, 102220 (2011); doi: 10.1063/1.3661991
View online: http://dx.doi.org/10.1063/1.3661991
View Table of Contents: http://scitation.aip.org/content/aip/journal/jap/110/10?ver=pdfcov
Published by the AIP Publishing

Interfaces in organic devices studied with resonant soft x-ray reflectivity

Hongping Yan,[1,a)] Cheng Wang,[2] Andres Garcia,[3] Sufal Swaraj,[1,4] Ziran Gu,[1] Christopher R. McNeill,[5] Torben Schuettfort,[5] Karen E. Sohn,[7] Edward J. Kramer,[6,7] Guillermo C. Bazan,[3,7] Thuc-Quyen Nguyen,[3] and Harald Ade[1]
[1]*Department of Physics, North Carolina State University, Raleigh, North Carolina 27695, USA*
[2]*Advanced Light Source, Lawrence Berkeley National Laboratory, Berkeley, California 94720, USA*
[3]*Department of Chemistry and Biochemistry, University of California, Santa Barbara, California 93106, USA*
[4]*Synchrotron SOLEIL, L'Orme des Merisiers, St Aubin Đ BP 48, Gif-sur-Yvette Cedex 91192, France*
[5]*Cavendish Laboratory, Department of Physics, University of Cambridge, J J Thomson Ave, Cambridge CB3 0HE, United Kingdom*
[6]*Department of Chemical Engineering, University of California, Santa Barbara, California 93106, USA*
[7]*Department of Materials, University of California, Santa Barbara, California 93106, USA*

(Received 1 October 2010; accepted 16 March 2011; published online 30 November 2011)

Interfaces between donor and acceptor semiconducting polymers are critical to the performance of polymer light-emitting diodes and organic solar cells. Similarly, interfaces between a conjugated polymer and a dielectric play a critical role in organic thin-film transistors. Often, these interfaces are difficult to characterize with conventional methods. Resonant soft x-ray reflectivity (R-SoXR) is a unique and relatively simple method to investigate such interfaces. R-SoXR capabilities are exemplified by presenting or discussing results from systems spanning all three device categories. We also demonstrate that the interfacial widths between active layers can be controlled by annealing at elevated temperature, pre-annealing of the bottom layer, or casting from different solvent mixtures. The extension of R-SoXR to the fluorine K absorption edge near 698 eV is also demonstrated. © *2011 American Institute of Physics*. [doi:10.1063/1.3661991]

INTRODUCTION

Conjugated semiconducting polymers and their applications have been attracting considerable attention in recent years. They are materials that are reshaping technologies, such as light emitting diodes (LEDs), solar cells (SCs), and thin-film transistors (TFTs), because of a tremendous interest in low-cost flexible electronics[1] and photovoltaic solar energy conversion.[1,2] Many of the organic semi-conducting materials can be processed from solutions, thus offering the potential for cost advantages. In all three classes of devices, the interface between constituent polymers is critically important, and a better understanding of the interfacial structure is required to better control the device performance.

In polymer LEDs (PLEDs), two different polymers are often used that allow greater flexibility in optimizing the injection and transport of electrons and holes. Laterally phase separated blends can be used for PLEDs, but polymer multilayers are frequently employed.[3–7] The fabrication of multilayer PLEDs is tremendously simplified with the use of charged conjugated polyelectrolytes (CPE). These are polar electron transport materials that can be cast from a polar solvent onto non-polar hole transport materials, such as poly[2-methoxy-5-(2′-ethylhexyloxy)-p-phenylene vinylene] (MEH-PPV). Various devices have been made using CPEs and MEH-PPV, but interfaces in CPE-based structures have not yet been characterized extensively.

A related but essentially reverse photo-physics to that of PLEDs occurs in polymer-based SCs.[8] A bound electron-hole pair, known as an exciton with a binding energy of ~0.4 eV, is created when a photon is absorbed. The exciton then diffuses and is required to reach an interface between two materials with different electron affinity and ionization potential. Exciton dissociation occurs via electron transfer from the donor to the acceptor material (or via hole transfer from the acceptor to the donor), and photocurrent is generated when these charges are separated and reach the device electrodes. Although many studies have been done with polymer/fullerene blends as active material[9,10] and the efficiency of fullerene-based devices is indeed higher than polymer/polymer devices,[11] the latter is still of interest, due to its higher open-circuit voltage and potential to create well-ordered nanostructures through the use of block-copolymers. Polymer/polymer devices in bilayer geometry also offer the advantage that the influence of the interfacial structure on device performance can be most readily measured and assessed.[12]

In TFTs, charge transport occurs essentially along a 1 nm deep accumulation layer in the semiconducting polymer at the interface with a dielectric layer.[13] Polymer dielectrics are being increasingly used in polymer TFTs, as they lead to less electron trapping[14] and allow for top gate devices to be fabricated via sequential solution deposition from orthogonal solvents. Besides molecular interactions, which determine the packing geometry of the semiconducting polymer, the charge transport performance is highly influenced by the microstructure of the film.[15] The surface and interfacial roughness is an important parameter when characterizing the microstructure. For example, the mobility of crystalline organic semiconductors is highly sensitive to the roughness of the surface of inorganic dielectric layers.[16–18]

[a)]Author to whom correspondence should be addressed. Electronic mail: hyan@ncsu.edu.

Despite the desirability for more in-depth structural knowledge, relatively little is known about the interfacial structure of organic devices and how it affects optoelectronic properties. Interfacial width, the root-mean-square (RMS) deviation of the physical roughness and chemical composition gradient normal to the interface, can be characterized by well-established techniques, such as neutron reflectivity (NR)[19,20] and x-ray reflectivity (XR). XR has been used extensively to investigate polymer thin films and their interfaces, including some organic devices.[21,22] Most of the time, however, the electron density contrast for polymers in conventional XR is rather small.[23,24] Neutron reflectivity has superior sensitivity to carbonaceous soft-condensed matter if one of the components is deuterated. This may be impractical or too expensive for many of the polymers used in organic devices, with materials costing up to $4,000 per gram, even if not deuterated. Consequently, only a very limited number of NR studies on optoelectronic relevant polymers have been carried out.[20,25,26] For fullerene-based devices, sufficient natural contrast exists for neutron scattering.[27,28] As an alternative, resonant soft x-ray reflectivity (R-SoXR) is a promising tool to characterize interfacial properties of organic thin films, due to high intrinsic material contrast that exists for most of the organic materials at soft x-ray energies.[29–33] Here, we present the use of R-SoXR to characterize the interfaces between active materials in all three categories of organic devices, i.e., polymer LEDs (PLED), polymer solar cells (PSCs), and polymer TFTs (PTFTs).

The assumption that the direct casting of the CPE layer on top of the MEH-PPV does not disrupt the MEH-PPV layer and that sharp interfaces are required for good performance of organic LEDs (OLEDs) was underlying the synthesis, development, and use of these CPE materials. Initial transmission electron microscopy (TEM) studies[34] have indeed shown that only materials of opposite polarity cast from solvents of matching polarity yield sharp interfaces and well-developed bilayer structures. Quantitative measurements of the interfacial width are, however, difficult with TEM, and the interface could only be characterized as being ~2 nm in width. Recent high precision R-SoXR studies on model bilayers have shown that the differential casting of CPEs on top of MEH-PPV yields sharp and smooth interfaces with an RMS width of 0.8 nm.[35] We extend these studies and show how the interfacial width can be controlled in bilayers by either the use of solvent mixtures for casting or a number of annealing protocols.

In addition, a detailed analysis of an almost complete OLED device consisting of a multilayer of PFNBr/MEH-PPV/poly(3,4 ethylene dioxythiophene): poly(styrenesulfonate)/indium tin oxide/glass (PEDOT:PSS/ITO/glass) substrate's structure is presented. The interfacial widths of all five interfaces in this device (without the top electrode) are quantitatively determined or estimated from R-SoXR data. A simplified and incomplete analysis of this multilayer has been reported previously.[24] It is demonstrated that the interfacial widths between the active CPE/MEH-PPV layers in the actual device are slightly larger than in the model bilayers. They are sufficiently similar to each other, though, that the more simple bilayer structures can be used as a proxy to investigate the influence of fabrication methods and procedures on the interfacial width between active layers.

The use of R-SoXR to study planar photovoltaic heterojunctions based on the polyfluorene co-polymers poly(9,9-dioctylfluorene-co-bis(N,N′- (4,butylphenyl))bis(N,N′-phenyl-1,4-phenylene)diamine) (PFB) and poly(9,9-dioctylfluorene-co-benzothiadiazole) (F8BT) is also discussed. By obtaining quantitative information of morphology, photoluminescence quenching, and device performance, it is possible to examine the competing effects of exciton and charge dissociation and to show that sharp, non-equilibrium interfaces produce the best device performance.[12]

The first R-SoXR results on TFT bilayers are presented. The devices consist of a dielectric top layer of either polystyrene (PS), poly (methyl methacrylate) (PMMA), or CYTOP CTL-809M (Asahi Glass) and a bottom layer of poly{[N,N′-bis(2-octyldodecyl)-naphthalene-1,4,5,8-bis(dicarboximide)-2,6-diyl]-alt-5-5′-(2,2′-bithiophene)} (P(NDI2OD-T2), Polyera Corporation). P(NDI2OD-T2) is a newly developed high-mobility electron transporting polymer.[36,37] Furthermore, the R-SoXR method can be successfully extended from the carbon 1s absorption edge to the fluorine 1s absorption edge.

EXPERIMENTAL METHODS

PFNBr/MEH-PPV bilayers and multilayer

MEH-PPV and PFNBr were synthesized following previously published protocols.[6] PEDOT:PSS (Baytron P) was used as received. The multilayer device was prepared on an ITO coated glass substrate (Thin Film Devices), onto which a ~6 nm thick PEDOT:PSS film was spun cast. The multilayer structure was completed by casting an ~80 nm MEH-PPV layer from toluene on the PEDOT:PSS, followed by spin casting a ~20 nm PFNBr layer from methanol. The nominal layer thicknesses are derived by spin casting single layers from the same solution and determining their thicknesses with an ellipsometer. Deposition of a metal cathode on top would complete this structure into an actual device.

PFNBr/MEH-PPV bilayers were prepared on SiO_2 substrates by casting an ~80 nm MEH-PPV layer first from toluene on the SiO_2 followed by spin casting a ~20 nm PFNBr layer from methanol or a tetrahydrofuran (THF):methanol solution. Methanol is a poor solvent for MEH-PPV, so the MEH-PPV layer surface should not be disturbed. In an attempt to disturb the smooth MEH-PPV surface during casting, a mixed solution with THF and methanol was used, because THF can dissolve both PFNBr (top layer) and MEH-PPV (bottom layer). Three different concentrations of THF were used (1%, 10%, 20% THF). To assess the effect of annealing, bilayers were annealed for 20 min at 150 °C and 230 °C, respectively.

Differences in annealing protocols were as follows from a different batch of materials: (1) direct casting of both layers without annealing; (2) casting and annealing at 230 °C of bottom MEH-PPV with subsequent casting of the PFNBr and no further annealing; and (3) differential casting of a bilayer with subsequent annealing at 230 °C. A complementary set of samples from this batch of materials was made as complete devices.

PFB/F8BT bilayers

Materials and sample preparation: PFB and F8BT were supplied by Cambridge Display Technology Ltd. and used as received. PFB had a molecular weight (M_w) and polydispersity (PDI) of 168 kg mol^{-1} and 2.8, respectively, while the M_w of F8BT was 190 kg mol^{-1} and PDI 1.9. Films were spin-coated from p-xylene with a thickness of typically 60 nm. PFB/F8BT bilayers were prepared by first spin casting F8BT onto the silicon wafer, and PFB was then spun cast onto a cleaned and oxygen plasma-treated glass slide and floated off onto de-ionized water. The F8BT-coated substrate was then lowered and laminated onto the air-side of the floating PFB film and picked up. Substrates were then placed overnight to dry in a vacuum chamber with pressure of less than 10^{-6} mbar. Samples were annealed by placing on a hotplate in the glovebox at the desired temperature for 10 min, and subsequently quenched to room temperature.

Dielectric/P(NDI2OD-T2) bilayers

P(NDI2OD-T2) was purchased from the Polyera Corporation, USA, and specified with a number average molecular weight (M_n) and polydispersity index (PDI) of 25.4 kg mol^{-1} and 4.03, respectively. The gate dielectrics poly(methyl methacrylate) (PMMA) and polystyrene (PS) with a weight average molecular weight (M_w) of 1000 kg mol^{-1} and 120 kg mol^{-1}, respectively, were purchased from Sigma-Aldrich. CYTOP CTL-809M was used as received from Asahi Glass. P(NDI2OD-T2) thin films were prepared by spin casting from a 20 g/l dichlorobenzene solution onto electron-conducting (antimony-doped) silicon wafers. The film thickness was determined using a profilometer (Veeco Dektak 3) to be around 55 nm. The P(NDI2OD-T2) films were subsequently annealed at 110 °C for 20 min in nitrogen atmosphere and quickly cooled to room temperature. Deposition of the gate material was also performed by spin casting from orthogonal solvents (n-butyl-acetate for PS and PMMA) using the same spin-conditions, which yielded a film thickness of 75 nm measured with the profilometer on a pristine silicon wafer. After deposition of the gate material, no further heat treatment was performed on the bilayers.

Data acquisition

Near edge x-ray absorption fine structure (NEXAFS) spectra of reference samples were acquired at beamline 5.3.2 at the Advanced Light Source (ALS).[38] These spectra are used to derive optical constants of the materials to predict contrast and provide initial optical constants for the fits and simulation.

R-SoXR data were acquired at beamline 6.3.2 at the ALS in a high vacuum ($\sim 10^{-7}$ Torr),[39] following previously established protocols.[31] To detect and avoid radiation damage, which can cause mass loss and spectral change,[40,41] some scans were repeated and the sample was occasionally translated to expose a fresh sample area. Simulations and fits were performed using the non-commercial program IMD.[42]

The R-SoXR data and fits sometimes show some discrepancy in the low q-region that has been traced to spectral contamination. The q range used to extract parameters from the fits is therefore sometimes restricted to ~0.2–2.5 nm^{-1}.[12]

RESULTS AND DISCUSSION

CPE/MEH-PPV bilayers

In order to employ simple sample preparation procedures and use the least complex R-SoXR analysis, a smooth silicon substrate was used instead of a relatively rough PEDOT:PSS/ITO/glass substrate for the majority of structures investigated. PFNBr/MEH-PPV/Si model bilayers were prepared by sequential casting from non-polar and polar solvents using established protocols. Methods to control the interfacial width were investigated by preparing PFNBr/MEH-PPV/Si bilayers by casting the PFNBr with 100% methanol or a THF:methanol mixture directly onto the MEH-PPV. In addition, PFNBr/MEH-PPV bilayers with PFNBr spun with 100% methanol were annealed at 150 °C and 230 °C for 20 min. MEH-PPV and PFNBr were also cast sequentially on PEDOT:PSS/ITO/glass substrates to simulate a complete device.

R-SoXR results at 285.6 eV of the PFNBr/MEH-PPV/Si bilayers cast from the different solvent mixtures are displayed in Fig. 1. Qualitatively, the reflectance profiles exhibit clear fringe modulations with two Δq's, indicating a bilayer structure. The quantitative results for the interfacial and surface widths, and the layer thicknesses from fits to the data in Fig. 1 are summarized in Table I. The interfacial width changed appreciably as a function of solvent polarity only for the highest THF content, i.e., the 20%:80% THF:methanol mixture. In this case, the width increases from 0.8 nm to 1.2 nm. The 1% and 10% THF solutions yield essentially the same sample as the use of a pure methanol solvent. These results are not unexpected. PFNBr has been specifically designed to allow differential casting from methanol, a poor solvent for MEH-PPV. The MEH-PPV layer surface is not disturbed much with the use of methanol, which has been previously demonstrated[35] and is confirmed

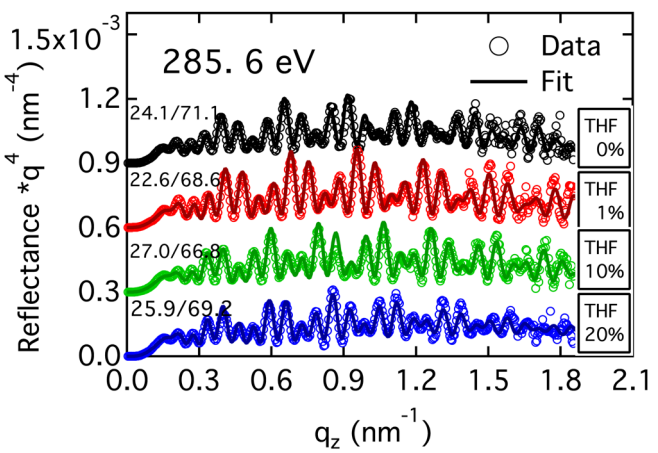

FIG. 1. (Color online) R-SoXR fits and data acquired at 285.6 eV for PFNBr/MEH-PPV bilayers, which had the PFNBr cast from methanol:THF mixtures as indicated. The numbers at the right of the reflectance traces are the layer thicknesses in nm as derived from the fits. Note the scaling by q^4.

TABLE I. Surface and interface roughness of PFNBr/MEH-PPV/Si bilayers and MEH-PPV reference layer as determined from fits shown in Figs. 1 and 2.

Sample	Surface Roughness RMS (nm)	Interfacial Roughness RMS (nm)
Standard	0.9	0.8
THF 1%	1.0	0.7
THF 10%	0.9	0.8
THF 20%	1.2	1.2
Annealed MEH-PPV single layer	1.7	
Bilayer with pre-annealed MEH-PPV layer	1.6	2.0
Annealed bilayer @150 °C	1.1	0.9
Annealed bilayer @230 °C	1.1	4.0

with the present results. Since THF can dissolve both PFNBr (top layer) and MEH-PPV (bottom layer), sufficient THF (i.e., 20%) during casting of the PFNBr does indeed broaden the interface.

The effect of different sample preparation procedures was also explored. In Fig. 2, R-SoXR results and fits of PFNBr/MEH-PPV bilayers prepared with the following procedures are plotted: direct casting without any further annealing (Fig. 2(b)), pre-annealing of the bottom MEH-PPV layer at 230 °C for 20 min, followed by casting the top PFNBr layer (Fig. 2(c)), and a bilayer made by direct casting both layers one-by-one and subsequent annealing of the entire bilayer at 230 °C (Fig. 2(d)). Clear, qualitative differences can be readily observed and interpreted: The more extensive the annealing and processing, the rougher the surface and interface. The quantitative values of surface and interfacial roughnesses from fits are summarized in Table I. As expected from the raw data, the surface and interfacial widths are greatly affected by the different sample preparation procedures and the interfacial roughness increases from 0.8 nm to 2.0 nm for the preannealed sample and to ~4 nm for the annealed bilayer. R-SoXR of an annealed single layer MEH-PPV sample is shown in Fig. 2(a) and yields a surface roughness of 1.7 nm. Previous R-SoXR results on as-cast MEH-PPV reported a very smooth surface with an RMS surface roughness of 0.52 nm and an increase of about 0.35 nm to 0.88 nm for the interfacial width upon casting of a PFNBr layer.[35] The present R-SoXR measurements thus indicate that the PFNBr/MEH-PPV interface further roughens slightly during the casting of the PFNBr, even for the preannealed MEH-PPV, with an increase of ~0.3 nm. This is very comparable to the increase observed for the as-cast MEH-PPV layer. Since the ~20 nm thin top layer is differentially spun cast onto a solid bottom layer, there would be no capillary waves during casting.[43] The present and prior results strongly suggest that the casting of the CPE does not significantly result in chemical interdiffusion and that the major contribution to the 2.0 nm width observed for the bilayer with a preannealed MEH-PPV bottom layer is due to the initial physical roughness of the MEH-PPV layer on which the PFNBr is cast. Whether or not there is a contribution from capillary waves to the roughness during the annealing of the entire bilayer is not relevant, as we are not interested in understanding thermodynamic interface properties, but the effects of processing on the interfacial width.

Figure 3 shows the R-SoXR data for the PFNBr/MEH-PPV/PEDOT:PSS/ITO/glass multilayer device at five photon energies. Complicated reflectance patterns arise as a function of photon energy, since the reflections from each interface interfere and their respective reflectivity is photon energy

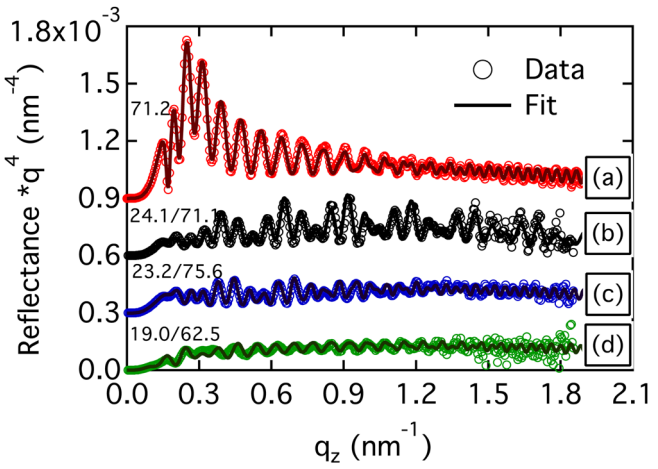

FIG. 2. (Color online) Reflectance acquired from (a) MEH-PPV single layer pre-annealed at 240 °C (270 eV), (b) as cast bilayer (285.6 eV), (c) as cast bilayer on pre-annealed MEH-PPV (285.6 eV), and (d) bilayer annealed at 230 °C. The numbers at the left of the reflectance traces are the layer thicknesses in nm as derived from the fits. Note the scaling by q^4. Data offset for clarity.

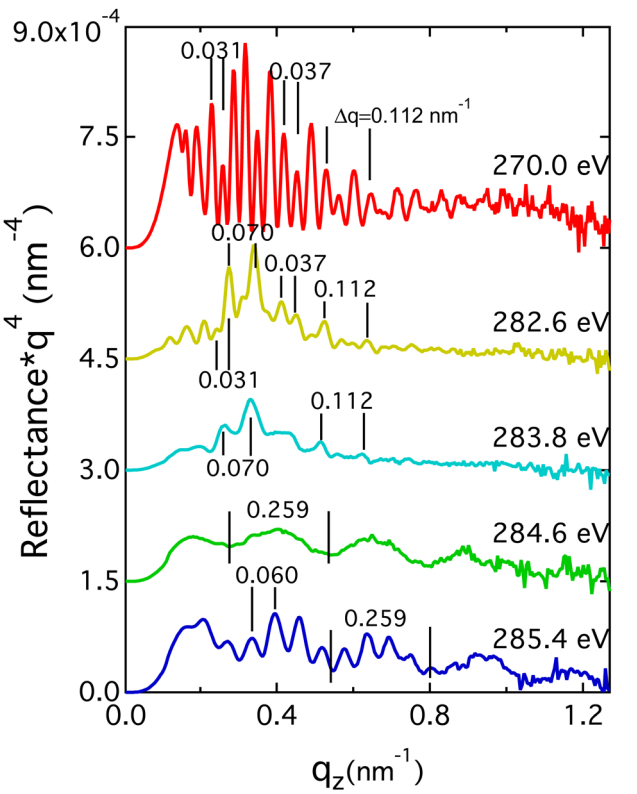

FIG. 3. (Color online) Reflectance of PFNBr/MEH-PPV/PEDOT:PSS/ITO/glass multilayer at selected photon energies. Note the scaling by q^4. Data offset for clarity.

TABLE II. R-SoXR sensitivity to particular interface and dominant fringe spacing of R-SoXR data of PFNBr/MEH-PPV/PEDOT:PSS/ITO/glass multilayer device (see Fig. 3) as a function of photon energy; nominal layer thickness, and quantitative results of layer thickness. Shaded areas indicate no particular sensitivity to this layer. Unit for Δq of fringes spacing is nm^{-1}.

		Semi-qualitative analysis from fringe spacing (nm)												
Photon energy		270.0 eV			282.6 eV				283.8 eV		284.6 eV	285.4 eV		
Interfaces observed		1,5	1,4	3,4	1,5	1,4	3,5	3,4	3,5	3,4	1,2	1,3	1,2	
Δq of fringes spacing		0.031	0.037	0.112	0.032	0.036	0.070	0.112	0.070	0.112	0.259	0.060	0.259	Fits/sim. (nm)
Layer	Nom. t (nm)													
PFNBr	25										24		24	23.5
MEH-PPV	80	203	172		196	175						104		78.8
PEDOT:PSS	60			56			90	56	90	56				60
ITO	30													30

dependent. In addition, absorption can play an important and dominant role in R-SoXR. Considering intrinsic materials contrast and taking absorption into account, the following picture can be deduced: (For simplicity, the vacuum/PFNBr, PFNBr/MEH-PPV, MEH-PPV/PEDOT:PSS, PEDOT:PSS/ITO, and ITO/glass interfaces will be referred to for the multilayer device as interface #1, #2, #3, #4, and #5, respectively.) At 285.4 eV, the top three interfaces have relatively strong reflections and the 4th and 5th interface is not efficiently probed, due to absorption. At 284.6 eV, interface #3 has very low contrast and relatively strong absorption in the MEH-PPV and PEDOT:PSS prevents probing of interfaces #4 and #5. Only interfaces #1 and #2 contribute. At 283.8 eV, interface #1 (the top surface) has a minimum in contrast. The contrast for the second interface is also low, yet this is an energy where there is little absorption and the third, fourth, and fifth interfaces are probed effectively. At 270 eV, primarily, interfaces #1, #3, #4, and #5 contribute. At 282.6 eV, primarily, interfaces #1, #4, and #5 are probed, with a minor contribution from interface #3. Hence, at these latter two energies, information about the total film thickness and the deeper interfaces is encoded in the complex reflectance profiles. Interface #2, at which charge combination and light emission occur, is most efficiently probed at 284.6 and 285.4 eV.

Having identified the contributing interfaces as a function of photon energy, the layer thickness of each layer can now be derived from the Δq's, as measured from the various fringe spacings indicated in Fig. 3. At 284.6 eV, there are only well-defined fringes with a Δq of approximately 0.259 nm^{-1}, corresponding to a derived thickness of $d \approx 2\pi/\Delta q = 24.2$ nm. At 285.4 eV, modulations of the Kiessig fringes corresponding to two Δq values are clearly visible, similar to those observed for polymer bilayers on Si substrates.[31,32] The smaller Δq equals ~ 0.060 nm^{-1} and corresponds to a thickness of ~ 104 nm. The larger $\Delta q = 0.259$ nm^{-1} yields the same information as the 284.6 eV data. A third Δq cannot be detected in the 285.4 eV data, directly indicating that only three of the five interfaces dominate this data. Photon energies of 282.6 eV and 270 eV yield dominant fringes with two different Δq's. For q values less than ~ 0.4 nm^{-1}, the average Δq is ~ 0.031 nm^{-1}, corresponding to a thickness of ~ 203 nm, while, for q values larger than that, the average Δq is ~ 0.037 nm^{-1}, corresponding to a thickness of ~ 170 nm. Furthermore, a regular pattern for higher q's is observed that corresponds to $\Delta q \approx 0.112$ nm^{-1}. At 283.8 eV, a $\Delta q \approx 0.070$ nm^{-1} is observed at low q, corresponding to a thickness of ~ 90 nm, and a $\Delta q \approx 0.111$ nm^{-1}, corresponding to ~ 56 nm, is observed at high q. The results of this analysis in conjunction with the dominant interface reflections are summarized in Table II. A self-consistent picture with only minor differences in layer thicknesses emerges. The average derived thicknesses for the top four layers are: ~ 24 nm, ~ 80 nm, ~ 56 nm, and ~ 30 nm, for a total of ~ 200 nm.

Through fits or simulations, one can extract more precise quantitative information for thicknesses and, more importantly, the interfacial widths from the various reflectance profiles. Figure 4 shows such fits or simulation for photon energies of 270, 284.6, and 285.4 eV, respectively. In contrast to the prior incomplete analysis,[24] a complete multilayer model was used here along with improved optical constants previously derived from independent measurements. Thickness, roughness, and optical constants can be fitted. The individual fits for the 284.6 eV and 285.4 eV reflectance yield a surface roughness of 0.9 nm and roughnesses of 1.1 nm and 3.5 nm for the PFNBr/MEH-PPV and the MEH-PPV/PEDOT:PSS interfaces, respectively. The layer thicknesses derived from the fits are 23.5 nm and 78.8 nm, in close agreement to the semi-quantitative estimates derived above. This is in agreement with prior fits using a simplified bilayer model.[24] Furthermore, the data at energies below 283.9 eV contains information about the interfacial widths or roughnesses of the PEDOT:PSS/ITO and the ITO/glass interfaces. For the 270 eV data, a complete fit over the full q range with all adjustable parameters is not converging, due possibly to some background and normalization issues in that data. Instead, we have used simulations for the 270 eV data that were visually optimized to match the Δq observed and the damping at the correct q. These simulations constrain the top three interfaces to those measured from the 284.6 eV and 285.4 eV data and use only measured optical constants. The only free parameters that are adjusted are the width of interfaces #4 and #5. These optimized simulations indicate that these interfaces have widths of 4.0 nm and 3.5 nm, respectively. The results of the fits and the simulation are

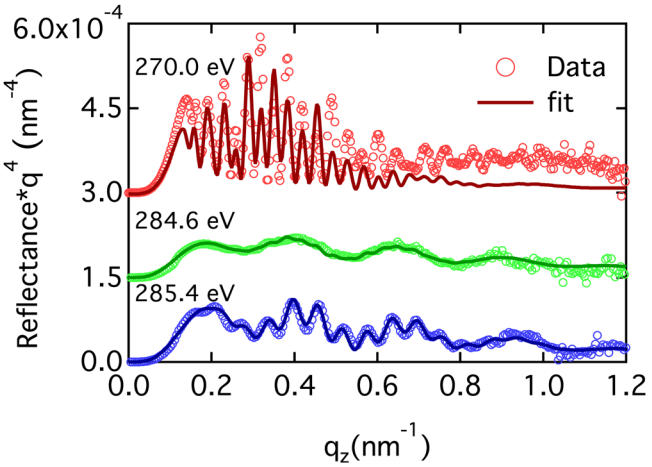

FIG. 4. (Color online) Fits of multilayer data 284.6 and 285. 4 eV and simulation of 270 eV data. Note the scaling by q^4. Data offset for clarity.

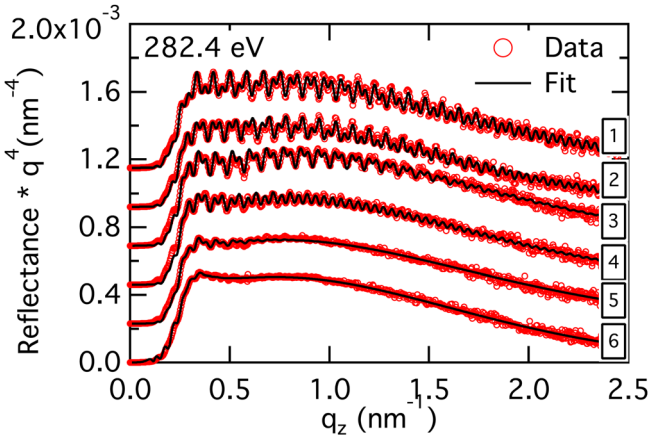

FIG. 5. (Color online) Representative R-SoXR data at 282.4 eV (open circle) and numerical fits (solid line) of Si/PFB/F8BT samples as a function of annealing. (1) As-prepared, (2) 100 °C, (3) 120 °C, (4) 140 °C, (5) 160 °C, and (6) 200 °C. The loss of the fringe modulations at higher annealing temperatures directly indicates an increase in polymer/polymer interfacial width. Note the scaling by q^4. Data offset for clarity.

summarized in Table II. In most experimental situations, one would often have enough processing flexibility to measure the surface roughness and any change in the first buried interfacial width after each processing step. We find it nonetheless interesting to use this multilayer sample as an example of what could be accomplished with R-SoXR if such flexibility did not exist or is operationally too complicated or time consuming.

Interestingly, the PEDOT:PSS/ITO interface (i.e., #4) is by far the roughest. Also, the width of the MEH-PPV/PEDOT:PSS interface is not significantly reduced from that observed for PEDOT:PSS/ITO. This implies that the casting of the PEDOT:PSS did not significantly smooth out the ITO roughness or that the PEDOT:PSS surface roughened during the casting of the MEH-PPV. The latter is relatively unlikely. By the time the last layer is cast, a very smooth surface of 0.9 nm is achieved. The CPE/MEH-PPV interface was rather sharp with a width of 1.1 nm. This is larger by ~0.2 nm than the width measured on bilayers cast on smooth substrates and must be caused by the larger initial roughness of the MEH-PPV in the multilayer. This difference is nonetheless relatively small compared to the overall width and, in particular, to the large changes in interfacial width observed as a function of annealing or even the 0.4 nm increase observed for 20% THF. Hence, the more simple bilayer structures can be used to characterize the interface as a function of sample preparation protocol, and any future correlation to device performance can be made from bilayer data and does not require the more complex analysis of the multilayers.

PFB/F8BT bilayers

Bilayer PFB/F8BT/Si heterojunctions were initially fabricated by floating, which minimizes material intermixing, and were subsequently annealed. Figure 5 shows the R-SoXR data acquired at 282.4 eV of such PFB/F8BT/Si bilayers. Fits of the reflectance profiles yield quantitative values for the width of the polymer/polymer interface and the surface. Table III summarizes the interfacial RMS roughness of average results for the interfacial width from at least three spots measured at 282.4 and 284 eV, at which the soft x-ray is sensitive to both the interface and the surface (180 °C data value from only two spots). As shown in the table, the as-prepared (no annealing), laminated bilayers have sharp interfaces with the 0.68 nm interfacial width consistent with the surface roughness of the initially spin-coated films. This value increases to 0.70 nm and 1.0 nm, even when the film is annealed at lowest temperatures of 100 and 120 °C, respectively. The interfacial widths quoted are averages from several spots, increasing the accuracy of the measurement. A discussion of the number of samples characterized and error analysis can be found in Ref. 12. When the films are annealed near or above the glass transition temperatures of the polymers (~140 °C), substantial increases in the interfacial width are observed, with a jump to 2.6 nm for 140 °C and ~6.7 nm for 200 °C.

In order to differentiate interface roughness from interface interdiffusion indirectly, surface roughness measurements on as-cast and 200 °C annealed single layer PFB and F8BT films were compared to the measured surface roughness of the bilayer films. As shown in Fig. 6, unannealed films are very sharp, with a surface roughness of ~0.46 nm for both F8BT and PFB. Annealing significantly roughened the surfaces, with measured roughnesses of ~1.8 nm for the

TABLE III. Fitting results from R-SoXR measurements of PFB/F8BT/Si bilayers at 282.4 eV and 284 eV, assuming an error function interface profile.

Sample	Interfacial root mean square (RMS) roughness (nm)
As-prepared	0.68
100 °C	0.70
120 °C	1.0
140 °C	2.6
160 °C	3.6
180 °C	6.5
200 °C	6.7

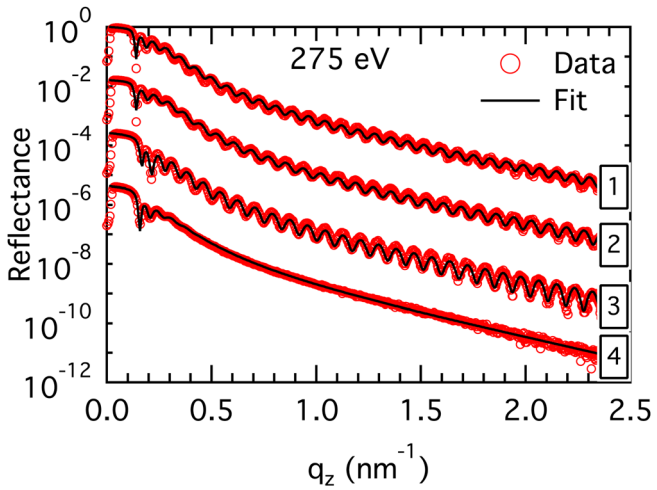

FIG. 6. (Color online) R-SoXR reflectance (open circle) and fits (solid line) of (1) PFB as-spun, (2) PFB 200 °C annealed, (3) F8BT as-spun, and (4) F8BT 200 °C annealed single layers. Data offset for clarity.

200 °C annealed PFB single layer, ~5.8 nm for the 200 °C annealed F8BT single layer, and ~6.7 nm for the 200 °C annealed Si/F8BT/PFB bilayer. The PFB surface roughness decreases with annealing to ~0.3 nm, annealing out features arising from casting.[31] Two important aspects are apparent: i) The bilayer surface, which has PFB on top, is rougher than the surface of the single layer PFB; and ii) the interface and surface roughnesses of the Si/F8BT/PFB bilayer have similar magnitude and are close to the single layer F8BT roughness. This strongly implies that F8BT roughens when annealed (presumably due to its liquid crystalline/semi-crystalline nature) and that this roughening determines the interface roughness and surface roughness in the Si/F8BT/PFB bilayer.[12]

A combination of R-SoXR characterization, J-V device data, photoluminescence quenching measurements, and Monte Carlo simulations revealed that only the sharpest interface yields the best device performance. The lower efficiency for the annealed device is attributed to decreased interfacial charge separation efficiency, which is partly due to a decrease in the bulk mobility of the constituent materials upon annealing, but also (and significantly) due to the increased interface roughness.[12] This could have profound implication for polymer/polymer device processing if the results are confirmed to be general for all polymer/polymer systems. New processing strategies that produce sharp non-equilibrium interfaces and increased use of block copolymers are indicated by these results.

Dielectric/P(NDI2OD-T2) bilayers

R-SoXR is successfully applied to dielectric/P(NDI2OD-T2) systems and extended to photon energies near the fluorine absorption edge at 698 eV.[44] Fig. 7 shows the reflectivity data at various energies of the following three systems: 1) PMMA on top of P(NDI2OD-T2); 2) PS on top of P(NDI2OD-T2); and 3) CYTOP (a fluorinated polymer) on top of P(NDI2OD-T2). The sensitivity of soft x-rays to the surface and interface of two polymers is clearly strongly

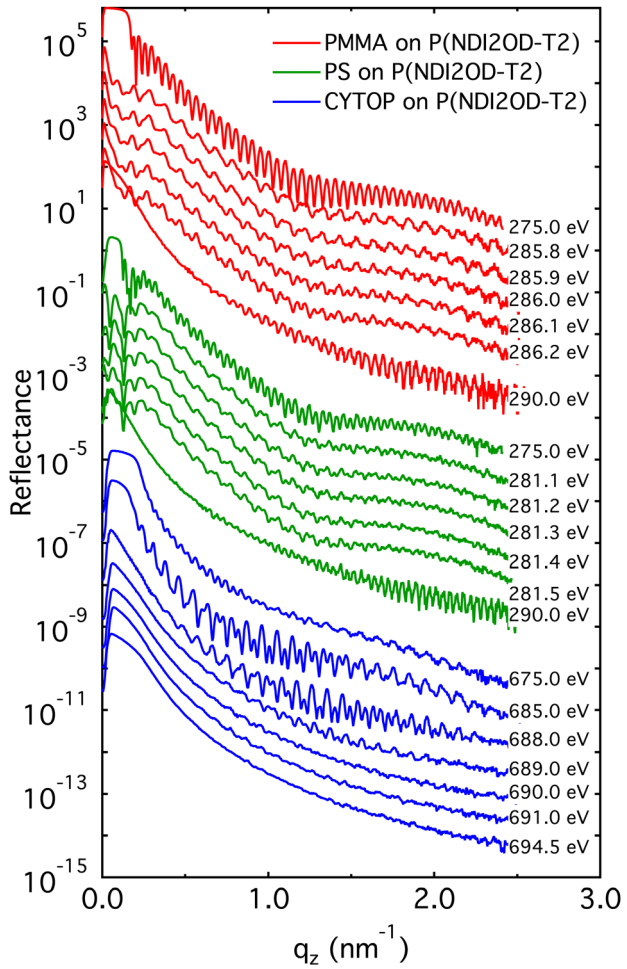

FIG. 7. (Color online) R-SoXR data acquired at a number of photon energies to show the selective sensitivity of the method to different interfaces for PS/P(NDI2OD-T2), PMMA/P(NDI2OD-T2), and CYTOP/P(NDI2OD-T2) bilayers at the carbon and fluorine absorption edges. Traces are offset for easy viewing. Data offset for clarity.

dependent on photon energy. At 275 eV, the total thickness of the bilayers is seen. In contrast to this, at 286 eV and 281.4 eV, the PMMA and PS surfaces are "turned off", respectively, and the bottom P(NDI2OD-T2) layer is probed almost exclusively. Significantly, R-SoXR also yields excellent tunable contrast near the fluorine absorption edge. As seen in Fig. 7, R-SoXR is very sensitive to the buried interface between CYTOP and P(NDI2OD-T2) at a photon energy around 688 eV. The slow modulation observed in the PS/P(NDI2OD-T2) and PMMA/P(NDI2OD-T2) bilayers arises from a thin silicon oxide layer of the substrates. Figure 8 shows some of these data along with a fit. By averaging at least three measured spots on each sample, we can derive the interfacial widths of the interfaces we are interested in. For PS/P(NDI2OD-T2) and PMMA/P(NDI2OD-T2) bilayers, the buried interface widths between polymers are measured to be 0.9 nm and 0.4 nm, respectively, with a surface roughness of 0.4 nm and 0.6 nm, respectively. For the CYTOP/P(NDI2OD-T2) bilayer, the surface and interface roughness are measured as 1.2 nm and 1.0 nm, respectively, around 285 eV(carbon edge). Fits to the reflectance acquired around 688 eV (fluorine edge) yield a surface

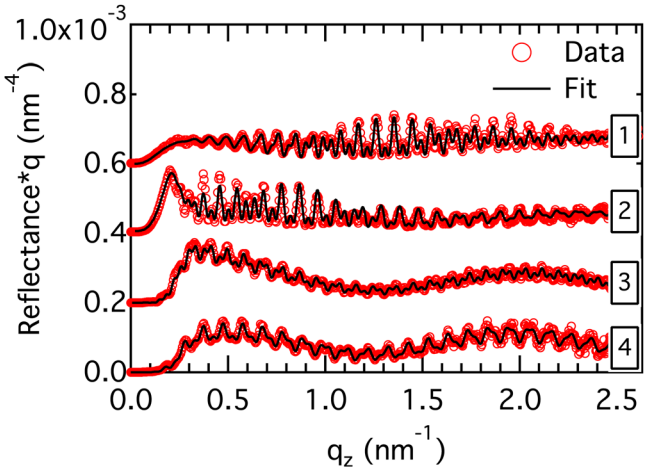

FIG. 8. (Color online) Data and fits for bilayers of: (1) CYTOP/P(NDI2OD-T2) at 688 eV; (2) CYTOP/P(NDI2OD-T2) at 285 eV; (3) PS/P(NDI2OD-T2) at 281.4 eV; and (4) PMMA/P(NDI2OD-T2) at 286.0 eV. Note that data and fits are scaled for better viewing in a single graph. Note the scaling by q^4. Data offset for clarity.

roughness of 1.0 nm and interface roughness of 1.1 nm. Considering that the C- and F-edge data are acquired at different spots on the same sample, the difference between measured results at the C-edge and the F-edge is likely due to variations across the sample. Variations between samples of nominally the same type and different locations on the same sample need to be assessed carefully before conclusions about relation to device performance can be drawn. The data here simply demonstrate that experimental conditions have been identified that allow now the various P(NDI2OD-T2)-based TFT systems and details of their processing to be assessed. Due to the very small interfacial width measured in some cases, the systematic influence of the substrate roughness to the error budget needs to be assessed further.

CONCLUSION

R-SoXR is a unique and productive complement to conventional XR and NR. For most materials systems investigated to date, there are photon energies experimentally accessible, at which sufficient contrast between materials exists to provide high quality data that will allow the quantitative determination of interfacial widths. Examples from three types of organic devices in which interfaces play a critical role have been presented.

The interfacial widths between active layers in a PFNBr/MEH-PPV optoelectronic device were shown to be tunable by annealing at elevated temperature, pre-annealing of the bottom layer, or casting from different solvent mixtures. Adding up to 20% THF to the PFNBr casting solution had the smallest effect. The interfacial width can be significantly broadened either by pre-annealing of the MEH-PPV bottom layer or post-annealing of a bilayer. The effects of sample preparation procedures on interfacial width can be readily characterized with R-SoXR, and comparison to device performance is now possible without having to deuterate one of the components.

Similarly for PFB/F8BT, it is shown that the interfacial width systematically increases with annealing temperature from 0.68 nm for pristine laminated bilayers to 6.7 nm with annealing at 200 °C. Combined with photoluminescence and device performance data, this study helps to partially explain the relatively poor efficiency of all-polymer systems. The results suggest that non-equilibrium, sharp interfaces are optimal for charge separation and that control of interface structure in solution-processed blends should be considered in order to maximize device efficiency. Novel processing routes and device fabrication processes that provide superior morphological control will have to be developed to harness the high V_{OC} potential exhibited by all-polymer devices.

Lastly, the R-SoXR method has been successfully applied to TFT bilayer systems consisting of the recently developed high-mobility electron-transporting polymer P(NDI2OD-T2). The interface roughness of the buried P(NDI2OD-T2) interface in PS- and PMMA-based bilayers has been measured. Furthermore, with results from the CYTOP/P(NDI2OD-T2) bilayer, we have demonstrated that R-SoXR has been extended from the carbon 1s edge to the fluorine 1s absorption edge.

ACKNOWLEDGMENTS

The authors are grateful for fruitful discussions with and help from E. Gullikson (CXRO), B. Watts, E. Gann, B. Collins, and T. Araki (NCSU). Work at NCSU was supported by the U. S. Department of Energy (DE-FG02-98ER45737). Work at UCSB was supported by the Materials Research Laboratory funded by the National Science Foundation under the MRSEC program (UCSB MRL, DMR-1121053), the NSF CAREER Award (DMR# 0547639), and the Department of Energy, Office of Basic Energy Sciences (DE-SC000-2368). K.E.S. was supported by a NSF Graduate Fellowship. Work at Cambridge was supported by the Engineering and Physical Sciences Research Council, U.K. (Advanced Research Fellowship EP/E051804/1). The authors thank Cambridge Display Technology Ltd. for supplying PFB and F8BT. Data were acquired at beamlines 5.3.2 and 6.3.2 at the ALS, which is supported by the Director of the Office of Science, Department of Energy, under Contract No. DE-AC02-05CH11231.

[1]*Organic Electronics. Materials, Manufacturing and Applications*, edited by H. Klauk (Wiley-VCH, New York, 2006).
[2]*Organic Photovoltaics: Concepts and Realization*, edited by C. Brabec, V. Dyakonov, J. Parisi, and N. S. Sariciftci (Springer, New York, 2003).
[3]J. Kido, M. Kimura, and K. Nagai, Science **267**, 1332 (1995).
[4]M. T. Bernius, M. Inbasekaran, J. O'Brien, and W. S. Wu, Adv. Mater. **12**, 1737 (2000).
[5]W. L. Ma, P. K. Iyer, X. Gong, B. Liu, D. Moses, G. C. Bazan, and A. J. Heeger, Adv. Mater. **17**, 274 (2005).
[6]X. Gong, S. Wang, D. Moses, G. C. Bazan, and A. J. Heeger, Adv. Mater. **17**, 2053 (2005).
[7]R. Yang, H. Wu, Y. Cao, and G. C. Bazan, J. Am. Chem. Soc. **128**, 14422 (2006).
[8]S. Gunes, H. Neugebauer, and N. S. Sariciftci, Chem. Rev. **107**, 1324 (2007).
[9]S. H. Park, A. Roy, S. Beaupre, S. Cho, N. Coates, J. S. Moon, D. Moses, M. Leclerc, K. Lee, and A. J. Heeger, Nature Photon. **3**, 297 (2009).
[10]W. L. Ma, C. Y. Yang, X. Gong, K. Lee, and A. J. Heeger, Adv. Funct. Mater. **15**, 1617 (2005).

[11]Y. Y. Liang, Z. Xu, J. B. Xia, S. T. Tsai, Y. Wu, G. Li, C. Ray, and L. P. Yu, Adv. Mater. **22**, 1 (2010).
[12]H. Yan, S. Swaraj, C. Wang, I. Hwang, N. C. Greenham, C. Groves, H. Ade, and C. R. McNeill, Adv. Funct. Mater. **20**, 4209 (2010).
[13]G. Horowitz, Adv. Mater. **10**, 365 (1998).
[14]L.-L. Chua, J. Zaumseil, J. F. Chang, E. C.-W. Ou, P. K.-H. Ho, H. Sirringhaus, and R. H. Friend, Nature **434**, 194 (2005).
[15]A. Salleo, R. J. Kline, D. M. DeLongchamp, and M. L. Chabinyc, Adv. Mater. **22**, 3812 (2010).
[16]S. E. Fritz, T. W. Kelley, and C. D. Frisbie, J. Phys. Chem. B **109**, 10574 (2005).
[17]M. L. Chabinyc, R. Lujan, F. Endicott, M. F. Toney, I. McCulloch, and M. Heeney, Appl. Phys. Lett. **90**, 233508 (2007).
[18]Y. Jung, R. J. Kline, D. A. Fischer, E. K. Lin, M. Heeney, I. McCulloch, and D. M. DeLongchamp, Adv. Funct. Mater. **18**, 742 (2008).
[19]R. A. L. Jones, *Polymers at Surfaces and Interfaces* (Cambridge University Press, New York, 1999).
[20]A. M. Higgins, S. J. Martin, M. Geoghegan, S. Y. Heriot, R. L. Thompson, R. Cubitt, R. M. Dalgliesh, I. Grizzi, and R. A. L. Jones, Macromolecules **39**, 6699 (2006).
[21]Y. J. Lee, H. Lee, Y. Byun, S. Song, J. E. Kim, D. Eom, W. Cha, S. S. Park, J. Kim, and H. Kim, Thin Solid Films **515**, 5674 (2007).
[22]Y. J. Lee, X. Li, D. Y. Kang, S. S. Park, J. Kim, J. W. Choi, and H. Kim, Ultramicroscopy **108**, 1315 (2008).
[23]O. H. Seeck, I. D. Kaendler, M. Tolan, M. Shin, M. H. Rafailovich, J. Sokolov, and R. Kolb, Appl. Phys. Lett. **76**, 2713 (2000).
[24]H. Ade, C. Wang, A. Hexemer, A. Garcia, T.-Q. Nguyen, G. C. Bazan, K. E. Sohn, and E. J. Kramer, J. Polym. Sci., Part B: Polym. Phys. **47**, 1291 (2009).
[25]A. M. Higgins, A. Cadby, D. C. Lidzey, R. M. Dalgliesh, M. Geoghegan, R. A. L. Jones, S. J. Martin, and S. Y. Heriot, Adv. Funct. Mater. **19**, 157 (2009).
[26]A. M. Higgins, S. J. Martin, P. C. Jukes, M. Geoghegan, R. A. L. Jones, S. Langridge, R. Cubitt, S. Kirchmeyer, A. Wehrum, and I. Grizzi, J. Mater. Chem. **13**, 2814 (2003).
[27]J. W. Kiel, A. P. R. Eberle, and M. E. Mackay, Phys. Rev. Lett. **105**, 168701 (2010).
[28]J. W. Kiel, M. E. Mackay, B. J. Kirby, B. B. Maranville, and C. F. Majkrzak, J. Chem. Phys. **133**, 074902 (2010).
[29]C. Wang, A. Hexemer, J. Nasiatka, E. R. Chan, A. T. Young, H. A. Padmore, W. F. Schlotter, J. Lüning, S. Swaraj, B. Watts, E. Gann, H. Yan, and H. Ade, IOP Conf. Ser.: Mater. Sci. Eng. **14**, 012016 (2010).
[30]H. Ade and A. P. Hitchcock, Polymer **49**, 643 (2008).
[31]C. Wang, T. Araki, B. Watts, S. Harton, T. Koga, S. Basu, and H. Ade, J. Vac. Sci. Technol. A **25**, 575 (2007).
[32]C. Wang, T. Araki, and H. Ade, Appl. Phys. Lett. **87**, 214109 (2005).
[33]S. Swaraj, C. Wang, T. Araki, G. Mitchell, L. Liu, S. Gaynor, B. Deshmukh, H. Yan, C. R. McNeill, and H. Ade, Eur. Phys. J. Spec. Top. **167**, 121 (2009).
[34]D. W. Steuerman, A. Garcia, M. Dante, R. Yang, J. P. Lofvander, and T. Q. Nguyen, Adv. Mater. **20**, 528 (2008).
[35]C. Wang, A. Garcia, H. P. Yan, K. E. Sohn, A. Hexemer, T. Q. Nguyen, G. C. Bazan, E. J. Kramer, and H. Ade, J. Am. Chem. Soc. **131**, 12538 (2009).
[36]H. Yan, Z. H. Chen, Y. Zheng, C. Newman, J. R. Quinn, F. Dotz, M. Kastler, and A. Facchetti, Nature **457**, 679 (2009).
[37]J. Rivnay, M. F. Toney, Y. Zheng, I. V. Kauvar, Z. Chen, V. Wagner, A. Facchetti, and A. Salleo, Adv. Mater. **22**, 4359 (2010).
[38]A. L. D. Kilcoyne, T. Tyliszczak, W. F. Steele, S. Fakra, P. Hitchcock, K. Franck, E. Anderson, B. Harteneck, E. G. Rightor, G. E. Mitchell, A. P. Hitchcock, L. Yang, T. Warwick, and H. Ade, J. Synchrotron Radiat. **10**, 125 (2003).
[39]J. H. Underwood and E. M. Gullikson, J. Electron Spectrosc. Relat. Phenom. **92**, 265 (1998).
[40]E. G. Rightor, A. P. Hitchcock, H. Ade, R. D. Leapman, S. G. Urquhart, A. P. Smith, G. Mitchell, D. Fisher, H. J. Shin, and T. Warwick, J. Phys. Chem. B **101**, 1950 (1997).
[41]T. Coffey, S. G. Urquhart, and H. Ade, J. Electron Spectrosc. Relat. Phenom. **122**, 65 (2002).
[42]D. L. Windt, Comput. Phys. **12**, 360 (1998).
[43]M. Sferrazza, C. Xiao, R. A. L. Jones, D. G. Bucknall, J. Webster, and J. Penfold, Phys. Rev. Lett. **78**, 3693 (1997).
[44]B. L. Henke, E. M. Gullikson, and J. C. Davis, At. Data Nucl. Data Tables **54**, 181 (1993).